Title

Interventional magnetic resonance imaging-guided cell transplantation into the brain with radially branched deployment.

Journal

Molecular therapy : the journal of the American Society of Gene Therapy, 23(1)

ISSN

1525-0016

Authors

Silvestrini, Matthew T
Yin, Dali
Martin, Alastair J
et al.

Publication Date

2015

DOI

10.1038/mt.2014.155

Peer reviewed

Interventional Magnetic Resonance Imaging-guided Cell Transplantation Into the Brain With Radially Branched Deployment

Matthew T Silvestrini[1,7], Dali Yin[1], Alastair J Martin[2], Valerie G Coppes[1,3], Preeti Mann[1,3], Paul S Larson[1,3], Philip A Starr[1], Xianmin Zeng[4], Nalin Gupta[1], S S Panter[1,3], Tejal A Desai[5], Daniel A Lim[1,3,6]

[1]Department of Neurological Surgery, University of California, San Francisco, San Francisco, California, USA; [2]Department of Radiology, University of California, San Francisco, San Francisco, California, USA; [3]Department of Surgery, Veteran's Affairs Medical Center, San Francisco, California, USA; [4]Buck Institute for Research on Aging, Novato, California, USA; [5]Department of Bioengineering, University of California, San Francisco, San Francisco, California, USA; [6]Eli and Edythe Broad Center of Regeneration Medicine and Stem Cell Research at UCSF, San Francisco, California, USA. [7]Present address: Department of Bioengineering, University of California, Davis, Davis, California, USA.

Intracerebral cell transplantation is being pursued as a treatment for many neurological diseases, and effective cell delivery is critical for clinical success. To facilitate intracerebral cell transplantation at the scale and complexity of the human brain, we developed a platform technology that enables radially branched deployment (RBD) of cells to multiple target locations at variable radial distances and depths along the initial brain penetration tract with real-time interventional magnetic resonance image (iMRI) guidance. iMRI-guided RBD functioned as an "add-on" to standard neurosurgical and imaging workflows, and procedures were performed in a commonly available clinical MRI scanner. Multiple deposits of super paramagnetic iron oxide beads were safely delivered to the striatum of live swine, and distribution to the entire putamen was achieved via a single cannula insertion in human cadaveric heads. Human embryonic stem cell–derived dopaminergic neurons were biocompatible with the iMRI-guided RBD platform and successfully delivered with iMRI guidance into the swine striatum. Thus, iMRI-guided RBD overcomes some of the technical limitations inherent to the use of straight cannulas and standard stereotactic targeting. This platform technology could have a major impact on the clinical translation of a wide range of cell therapeutics for the treatment of many neurological diseases.

Received 14 July 2014; accepted 9 August 2014; advance online publication 16 September 2014. doi:10.1038/mt.2014.155

INTRODUCTION

For cell-based therapies, successful translation of preclinical animal research into clinical practice requires cell delivery devices and methodologies that are effective at the scale and complexity of the human patient.[1–3] Due to its blood–brain barrier, delicate nature, and complex anatomy, the brain presents difficult challenges to the delivery of cell therapeutics.[3] While much recent translational research has been focused on improving the quality and quantity of human cell types for transplantation,[4] there has been very little innovation of the surgical tools and techniques used for cell delivery to the human brain.[5–11] If unresolved, faults with cell delivery may contribute to the failure of clinical trials despite robust preclinical evidence and a compelling biological rationale.

In past and ongoing clinical trials, cells have been transplanted into the human brain with rigid, straight metal cannulas coupled to a syringe.[8,12–16] While effective for the relatively small brain targets of animal experimental models, straight cannulas can be problematic when used at the scale and complexity of the human brain.[3] For instance, a common approach to translational scale-up involves increasing the number of brain penetrations,[8,12–16] and each independent cannula insertion injures normal brain tissue and may result in complications such as hemorrhagic stroke.[17–19] While convection enhanced delivery can greatly increase the dispersal of gene therapy vectors and drugs administered through a straight cannula,[20–22] this procedure does not increase the distribution of cells, as they are too large to be "pushed" through the interstitial spaces of brain parenchyma.[3]

An additional challenge relates to the shortcomings inherent to standard stereotaxy—a method of targeting nonvisualized anatomic structures by use of a three-dimensional coordinate system (see **Supplementary Figure S1**). The three-dimensional coordinates are generally derived from a preoperative volumetric MRI brain scan that is spatially registered to a frame or skull-mounted aiming device. This allows the insertion of a cannula through a small cranial burr hole along a precise, single trajectory to a specific, predetermined coordinate inside the skull. However, since MRI scans are not obtained during the procedure, the exact anatomic position of the cannula cannot be confirmed, which can lead to suboptimal accuracy of cell delivery and even "missed" targets.[23] Sources of such targeting error include brain "shift" within the skull due to loss of cerebrospinal fluid during surgery,[24]

Correspondence: Daniel A Lim, Department of Neurological Surgery, University of California, San Francisco, 35 Medical Center Way, RMB 1037, San Francisco, CA 94143-0112, USA. E-mail: LimD@neurosurg.ucsf.edu

inaccuracies in the registration of MRI images with the targeting device, and mechanical imprecision of the targeting device itself.[25]

Interventional magnetic resonance image (iMRI) is a recent technology that enables "real-time" imaging of stereotactic neurosurgical procedures.[26] With iMRI, the target is identified immediately before cannula insertion, which enables corrections for intraoperative brain shift, and "live" images during device insertion are obtained to confirm accurate cannula insertion to the anatomic target. iMRI has proven to be an effective method for the placement of deep brain stimulation (DBS) electrodes inserted through a straight cannula,[27–30] and iMRI procedures can now be performed in the common 1.5 Tesla (T) diagnostic scanner available in most hospitals.[25]

We recently described a metal device prototype that enables the radially branched deployment (RBD) of a cell delivery catheter at multiple points along a cannula tract.[11] By varying the depth, rotation, and radial distance of catheter deployment, one could use RBD to deliver cells in a customizable "tree-like" pattern branched from a single cannula insertion. iMRI would facilitate RBD-based delivery to anatomically large and/or complex brain target regions, as the delivery could be monitored with real-time imaging, and transgression of critical brain structures could be more precisely avoided.

Here, we have developed and tested an iMRI-guided RBD system intended for clinical use. RBD device components were fabricated with MRI-compatible, medical-grade materials. To lower the barriers to its clinical implementation, we integrated RBD with an US Food and Drug Administration (FDA)–approved iMRI skull-mounted aiming device and targeting software. All elements have been designed to ensure practical "usability" and enhance patient safety. By overcoming limitations inherent to the use of straight cannulas and standard neurosurgical stereotaxy, iMRI-guided RBD may be an important tool for the successful translation of cell therapy for many diseases of the brain.

RESULTS

Development of an iMRI-compatible RBD system

To enable the use of RBD with iMRI, we fabricated all components with MRI-compatible materials (**Table 1**). All device materials were medical grade, and the components were assembled in an EN ISO 13485:2003 certified facility. The iMRI-compatible RBD system consisted of three major subassemblies: the guide cannula, the delivery catheter, and the positioning collet (**Figure 1a–c**). Briefly, these subassemblies were designed to integrate and function in the following manner (**Figure 1d,e**): (1) the positioning collet attaches to an MRI-compatible aiming platform, which determines the initial guide cannula trajectory into the brain parenchyma; (2) the positioning collet provides control over the depth and radial angle of the guide cannula, which has a single distal side port; (3) the delivery catheter containing the desired cell dose is inserted and locked into the guide cannula; (4) proximal control elements open the guide cannula side port and deploy the delivery catheter along a known radial path; (5) advancement of the plunger wire delivers the cell dose to this radial target location; (6) the delivery catheter is then retracted, the side port closed, and the catheter can then be exchanged for another containing a second dose of cells; (7) controls on the positioning collet bring the guide cannula side port to a new depth and/or radial angle for catheter deployment and cell delivery; (8) steps (3–7) above can be repeated to deliver cellular deposits to multiple locations at various radial distances, angles, and depths along the guide cannula tract.

The iMRI-compatible RBD guide cannula subassembly was comprised of an outer guide tube and an inner guide tube that assembled in a nested manner (**Figure 2a**). Guide cannulas are commonly used in stereotactic procedures, such as the implantation of DBS electrodes, and these are generally made of stainless steel. Despite being fabricated of MRI-compatible materials, the outer diameter of the iMRI RBD guide cannula (**Table 1**) was up to 8% smaller than the metal cannulas used for DBS (**Supplementary Table S1**).

The delivery catheter subassembly was comprised of a catheter with two side infusion ports and a plunger wire that translates within the catheter lumen (**Figure 2b**). The delivery catheter outer diameter (**Table 1**) was the same or up to 30% smaller than cell delivery cannulas recently used for transplantation into the human brain (**Supplementary Table S1**). The distal end of the solid Nitinol plunger wire was attached to a tapered segment of Nitinol coil for increased flexibility, and the distal tip incorporated a Kynar piston with polyurethane leaflets (**Figure 2c**) that formed a gas-tight seal within the catheter lumen. When advanced to the most distal end, the plunger wire displaced nearly all of the volume within the catheter lumen (**Figure 2d**). After the delivery catheter was "backfilled" with fluid, advancement of the plunger wire delivered precise volumes directly proportional to the distance of plunger travel (1.08 µl ± 0.15 µl per cm of plunger travel; n = 25 trials), which represents a degree of precision similar to that achieved by manually operated Hamilton microsyringes.[31] Thus,

Table 1 RBD materials and dimensions

Subassembly	Part name	Proximal control elements	Body/distal end	Overall length (cm)	OD (mm)	ID (mm)
Guide cannula	outer guide tube	Accura 60	PEEK	30	1.57	1.06
Guide cannula	inner guide tube	Accura 60	Nylon-12	33.4	1	0.74
Delivery catheter	Catheter	Nylon-12	Nylon-12	41.7	0.64	0.38
Delivery catheter	plunger wire	Nitinol	Nitinol coil, Kynar (PVDF) tip, polyurethane leaflet valves	47.5	0.38	N/A
Positioning collet	N/A	Accura 60	Accura 60	N/A	N/A	N/A

ID, inner diameter; N/A, not applicable; OD, outer diameter; RBD, radially branched deployment.

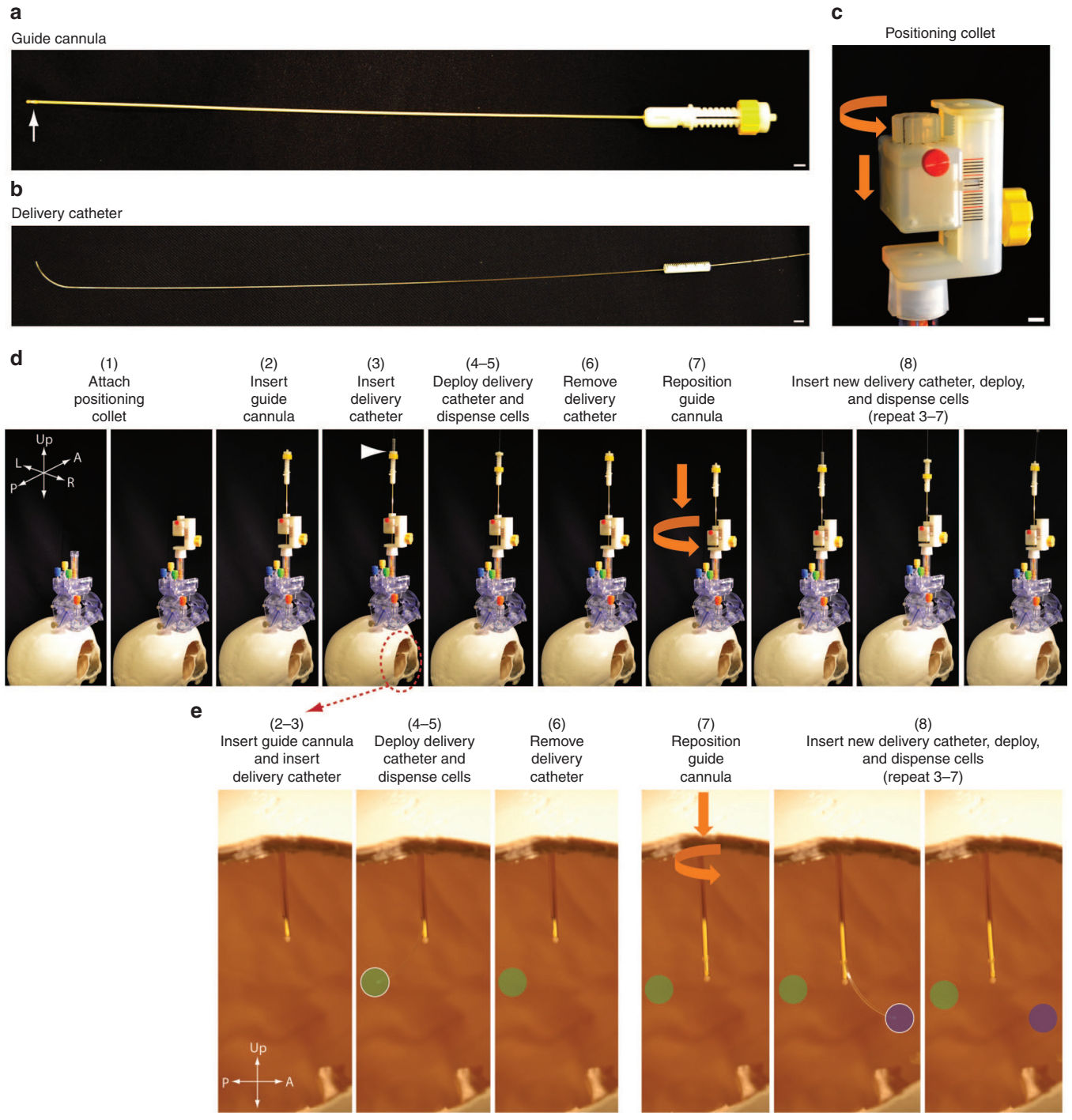

Figure 1 Overview of the iMRI-guided RBD platform. (**a**) Guide cannula with distal side port (white arrow, left) and proximal controls (right). (**b**) Delivery catheter with dual side infusion ports (not seen at this magnification) at the curved distal end (left) and the proximal locking hub (right). A plunger wire is fitted into the catheter lumen. (**c**) Positioning collet. Orange arrows indicate the rotational (radial angle) control provided by the white hub (top) and depth control provided by the yellow wheel (right). Horizontal markings (black and red lines, mm spacing) indicate changes in collet depth. Scale bars = 5 mm. (**d**) RBD use illustrated with a human skull model. View is from the posterior right. The RBD platform was mounted over a right frontal burr hole. (1) Attachment of positioning collet to the MRI-compatible, skull mounted aiming device; (2) insertion of guide cannula through the positioning collet; (3) insertion of delivery catheter with the proximal hub locking into the guide cannula proximal controls (white arrowhead); (4) deployment of the catheter through the opened guide cannula side port; (5) delivery of cells with plunger wire; (6) removal of delivery catheter and closure of the guide cannula side port; (7) repositioning of guide cannula side port to new depth and radial angle; (8) delivery to new location via repetition of (3–7). (**e**) Intracranial view of RBD action. The skull in **d** had a right-sided pterional craniotomy, and this window was used for intracranial observation. Numbering above each panel corresponds to those in **d**. (2–3) insertion of guide cannula containing a cell delivery catheter; (4–5) depoloyment of delivery catheter and delivery of cells, schematized as a green circle; (6) removal of delivery catheter and closure of the guide cannula side port; (7) repositioning of the side port to a new depth and radial angle; (8) delivery of cells schematized as a purple circle. Note that radial deployment can be performed at shorter distances (closer to the guide cannula), as needed. iMRI, interventional magnetic resonance imaging; RBD, radially branched deployment.

the iMRI-compatible delivery catheter performs as both a delivery cannula and precision microsyringe.

The RBD guide cannula and delivery catheter subassemblies contained multiple design elements to control radial deployment of the catheter through the guide cannula side port. After insertion of the delivery catheter into the proximal lumen of the guide cannula, the cylindrical hub of the delivery catheter was "captured" by the proximal screw drive mechanism (**Figure 2e,f**). Rotation of the proximal control arm opened the distal side port, exposing the lumen and angled deflector of the inner guide tube (**Figure 2f**). Manual clockwise rotation of the screw drive wheel resulted in advancement (1 mm per turn of the wheel) of the cell delivery catheter, which was observed as linear hub movement at the proximal end (**Figure 2g**). Through the combined action of the deflected bore tip of the inner guide tube and the J-shape distal curve (radius of curvature = 10.03 mm) of the delivery catheter, this linear movement was converted into radial catheter deployment along a smoothly curved path (**Supplementary Figure S2**). The screw drive provided 19 mm of translational movement of the catheter, which was converted into ~12 mm of radial distance, and by monitoring its deployment via markings on its proximal hub (**Figure 2f,g**), the location of the catheter tip could be determined (**Table 2**).

To measure the precision of iMRI RBD catheter deployment, we analyzed the reproducibility of catheter location when deployed into a gel that mimics the biomechanical properties of brain tissue. Two cameras positioned orthogonal to the guide cannula side port were used to document the deployment of 25 delivery catheters each into fresh brain tissue mimics. At both half and full deployments, the precision of catheter location was submillimetric (**Supplementary Table S2**). As the clinical precision of current stereotactic platforms is > 1.0 mm,[32,33] the mechanical performance of iMRI RBD catheter deployment is compatible with clinical use.

To facilitate the delivery of different cell doses (or cell types) to different locations, we designed the delivery catheter to be a

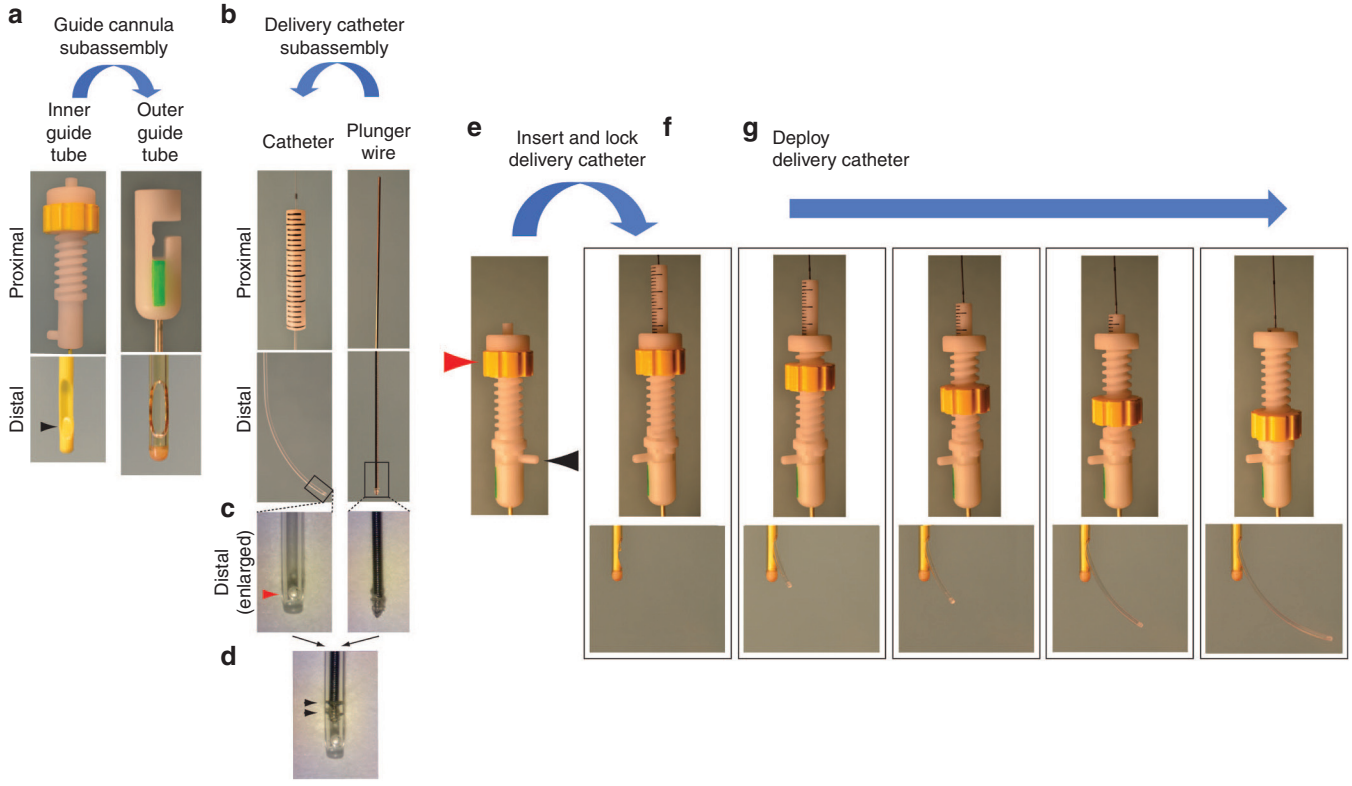

Figure 2 Guide cannula and delivery catheter subassemblies. (**a**) The inner guide tube was fitted into the outer guide tube (blue arrow) to form the guide cannula subassembly. The distal end of the inner guide tube had a side port with a distal deflector tip (black arrowhead), and the outer guide tube had an oval side port near the blunt distal end. (**b**) The delivery catheter subassembly was comprised of a catheter and a plunger wire fitted into the catheter lumen (blue arrow). A hub with 1 mm markings was attached to the proximal end of the catheter, and the proximal plunger wire was comprised of solid Nitinol, for stiffness. The distal end of the catheter was set with a curve, and the distal portion of the plunger wire was comprised of a Nitinol coil, for flexibility. (**c**) Enlarged views of the distal catheter and plunger wire. The catheter had two side infusion ports (red arrowhead) near the blunt catheter tip, and the plunger wire had a PVDF tip with dual leaflets to form a seal when inserted into the catheter lumen. (**d**) Plunger wire inserted to the distal end of the catheter. Dual leaflets forming the seal (black arrowhead) are seen near the side infusion ports. Component dimensions are in Table 1. (**e–g**) Radial catheter deployment. (**e**) Proximal end of the guide cannula without a delivery catheter. The yellow wheel (red arrowhead) controlled catheter radial deployment, and the white arm (black arrowhead) opened and closed the distal side port. (**f**) Insertion of delivery catheter and locking of its proximal hub into the radial deployment control wheel of the guide cannula subassembly. (**g**) Deployment of the delivery catheter via clockwise rotation of the radial deployment control wheel. Top panels: linear translational advancement was monitored by mm markings on the delivery catheter proximal hub. Bottom panels: linear translational movement resulted in radial deployment of the delivery catheter along a curved path. Location of the catheter tip was measured and is reported in **Table 2**. Precision of catheter deployment is reported in **Table 1** and illustrated in **Supplementary Figure S2**.

modular, exchangeable component. Counterclockwise rotation of the screw drive wheel resulted in the smooth retraction of the delivery catheter (not shown), and after closure of the side port, the catheter can be fully removed from the guide cannula and replaced with another.

RBD requires control over the radial angle of the guide cannula, but this degree-of-freedom is not controlled by standard stereotactic platforms. Furthermore, in current neurosurgical stereotaxy, guide cannula insertion depth is generally determined by a rudimentary depth stop collar, making smooth, gradual adjustments to this stereotactic parameter difficult. To provide mechanized control over both radial angle and depth of the RBD guide cannula, we developed the positioning collet subassembly, which was designed to function as an "add-on" component to a standard neurosurgical stereotactic platform. The present version attached securely but reversibly to the SmartFrame (**Figure 1d**), an FDA-approved, MRI-compatible skull-mounted cannula-aiming device. After the guide cannula was inserted into the collet, the radial angle and depth were governed by intuitive control elements. Rotation of the positioning collet hub changed the rotational angle of the guide cannula side port (**Figure 1d**,**e**, **Supplementary Figure S3**). The collet hub incorporates a rotation lock (small red knob, **Supplementary Figure S3b,c**) that prevents inadvertent rotation of the guide cannula. Rotation of the positioning collet wheel (yellow knob) resulted in gradual changes of the side port depth (**Figure 1d**,**e**). Thus, this novel iMRI-compatible positioning collet provides control over stereotactic parameters that leverage the utility of radial catheter deployment.

Table 2 Location of catheter tip at different radial deployments

Proximal marking (mm)	Y distance (mm)		Z depth (mm)	
	Mean	SD	Mean	SD
2	0.6	0.06	N/A	N/A
4	1.09	0.15	0.13	0.22
6	1.99	0.28	1.78	0.51
8	3.15	0.33	3.56	0.4
10	4.26	0.35	4.89	0.19
12	5.51	0.61	6.19	0.19
14	7.65	0.49	7.33	0.27
16	9.31	0.51	8.39	0.36
18	11.34	0.52	8.72	0.03
19	12.44	0.31	8.87	0.09

$n = 3$ for all the SD calculations.
N/A, not applicable.

Integration of iMRI-guided RBD with a clinically relevant workflow

To evaluate the function of the iMRI-compatible RBD device for delivery into the brain of a large animal model, we performed procedures in Yorkshire swine ($n = 7$; **Supplementary Table S3**). There were no surgical complications in this series, and no animals showed any signs of neurological deficits postoperatively. All surgical tools and operative strategies were essentially the same as those used for human stereotactic neurosurgical procedures. Briefly, with the animal under general anesthesia, we created a small scalp incision, a 12 mm burr hole, and then a small opening in the dura and pia mater (**Figure 3a**). Next, the SmartFrame aiming device was mounted to the skull (**Figure 3b**) and affixed with the positioning collet. For procedures with iMRI guidance, high-resolution images were obtained with a clinical 1.5T diagnostic MRI scanner (**Figure 3c**,**d**; MRI scanning parameters in **Supplementary Table S4**), and surgical planning was performed on a computerized workstation. The guide cannula trajectory

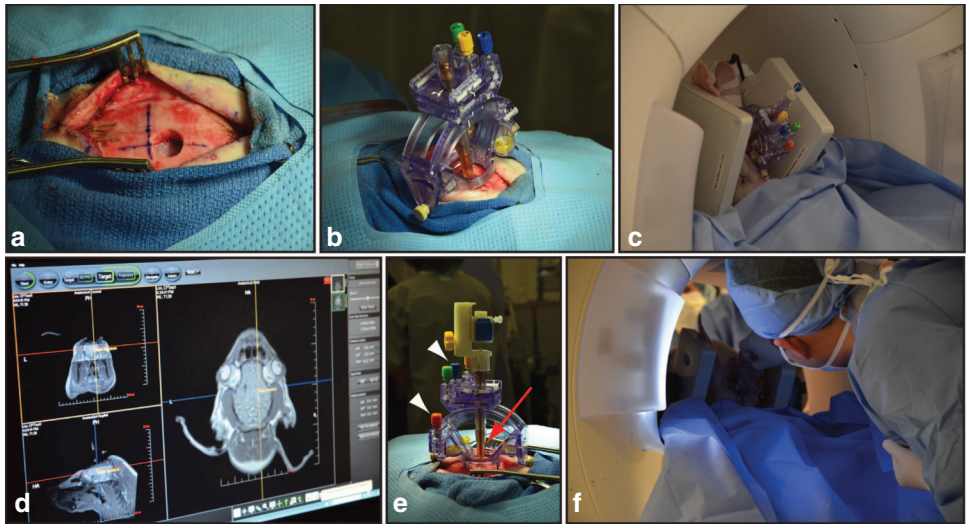

Figure 3 iMRI-guided RBD function in a clinically relevant neurosurgical workflow. (**a**) Burr hole in the right frontal swine skull. A small opening in the dura and pia mater was made before mounting the aiming device. (**b**) iMRI-compatible aiming device mounted over the burr hole. (**c**) Swine head with iMRI-compatible platform in the bore of a clinical 1.5T diagnostic MR scanner. (**d**) Example of neurosurgical planning with MRI data acquired very shortly before intracerebral delivery. (**e**) Adjustments to pitch and roll controls (white arrowheads) on the skull-mounted aiming platform to align the fluid-filled guide stem (red arrow) with the planned guide cannula trajectory. (**f**) Insertion of the guide cannula and conduct of the RBD procedure, shown in more detail in **Figure 1**. iMRI, interventional magnetic resonance image; RBD, radially branched deployment.

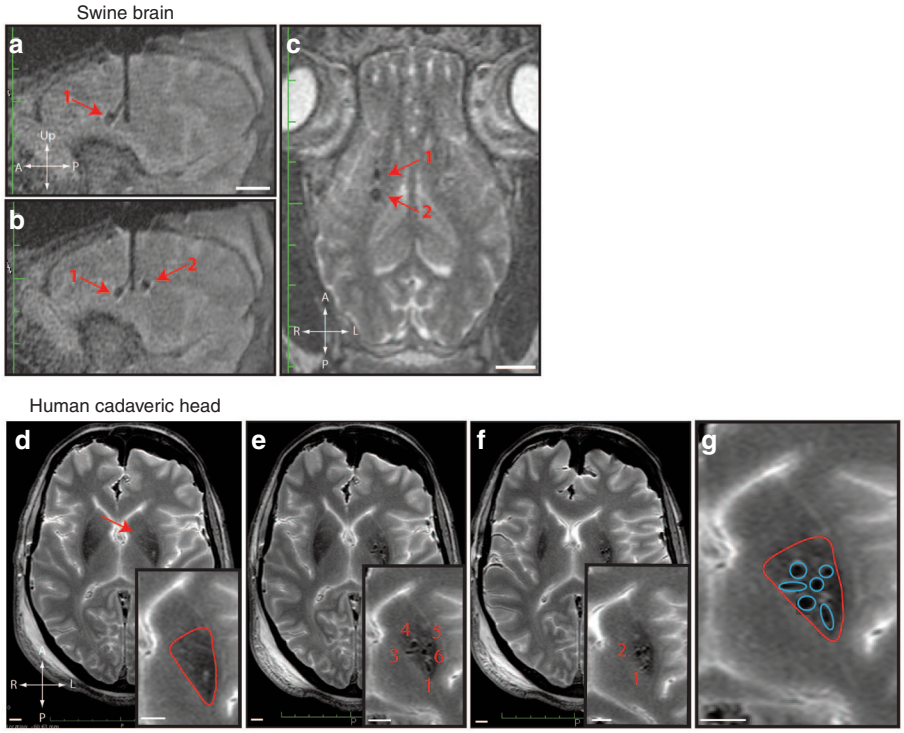

Figure 4 iMRI-guided RBD delivery of SPIO to multiple radial locations via a single guide cannula insertion. (**a–c**) SPIO delivery to the swine brain striatum. (**a,b**) Sagittal MRI images (anterior is left). (**a**) First SPIO delivery (1) to the anterior striatum. (**b**) Second SPIO delivery (2) posterior and 4 mm superior to the first. (**c**) Axial MRI taken after guide cannula removal showing the anterior (1) and posterior (2) SPIO deposits. (**d–g**) Axial MRI images of SPIO delivery to the human cadaveric putamen. (**d**) Before SPIO delivery. Arrow indicates the region of the putamen, which is shown enlarged and outlined in the inset at the lower right. (**e,f**) After six deliveries of SPIO (numbered in red) via a single guide cannula insertion. The two panels show different axial planes to illustrate the different radial and depth locations of the SPIO deposits. (**g**) Enlarged view of the putamen (red outline) with the regions of the SPIO deposits (blue outline). White scale bars = 1 cm. iMRI, interventional magnetic resonance image; RBD, radially branched deployment; SPIO, super paramagnetic iron oxide.

was determined by integrating the location of our desired targets with the RBD catheter deployment characteristics (**Table 2**), and MRI data were used to avoid transgression of major blood vessels, cortical sulci, and the cerebral ventricles. With imaging feedback obtained from rapid MRI scans, mechanical adjustments to the aiming device were made to match the bore of the fluid-filled targeting stem with the intended guide cannula trajectory (**Figure 3e**). The guide cannula was then inserted and advanced to the first position with the positioning collet (**Figure 3f**).

To visualize delivery with MRI, we injected a suspension of super paramagnetic iron oxide (SPIO) beads. With iMRI-guided RBD, SPIO was delivered to the anterior striatum (**Figure 4a**), and **a** second delivery was targeted 180° posterior and 4 mm superior (**Figure 4b**) with respect to the first. MRI scans performed after the injections confirmed this intended pattern of delivery (**Figure 4c**). No reflux of the 10 µl SPIO suspension was observed. After the postdelivery MRI scans, the RBD device and SmartFrame were removed, the burr hole and scalp closed, and the pig was extubated and allowed to recover under observation. Thus, the iMRI-guided RBD platform functions within a clinically relevant, neurosurgical workflow.

iMRI-guided RBD function at the scale of the human brain

The human brain is ~7 times larger than that of the pig.[34] To determine whether the iMRI-guided RBD device functions at the scale of the human brain, we performed procedures with human cadaveric heads (n = 3; **Supplementary Table S5**). Using standard neurosurgical techniques, we mounted the SmartFrame with positioning collet over a frontal skull burr hole. The putamen is a 3.6 cm^3 brain region[35] that becomes dopamine neuron denervated in patients with Parkinson's disease (PD) and has been the site of cell transplantation therapy. After surgical planning with iMRI (**Supplementary Table S6**), the guide cannula was inserted to the putamen along the prescribed path, which did not transgress any sulci or the ventricles. From this single cannula axis, based on the known RBD device characteristics (**Table 2**), SPIO deposits were delivered to the putamen with multiple catheter deployments at various planned radial angles and depths (**Figure 4d–g**). These data indicate that iMRI-guided RBD can facilitate delivery to a relatively large, clinically relevant brain target via a single guide cannula insertion.

Delivery of hESC-derived dopamine neuron precursors with iMRI-guided RBD

To evaluate the utility of iMRI RBD for the delivery of neural cells, we first evaluated cell viability after transit through the cell delivery catheter. Murine neural stem cells at a wide range of concentrations (1–8 × 10^7 cells/ml) had high viability before (98.7 ± 0.6% SD) and after (98.4 ± 0.4% SD; n = 9; t-test P = 0.29) transit as assessed by flow cytometric quantification of Sytox Red uptake.

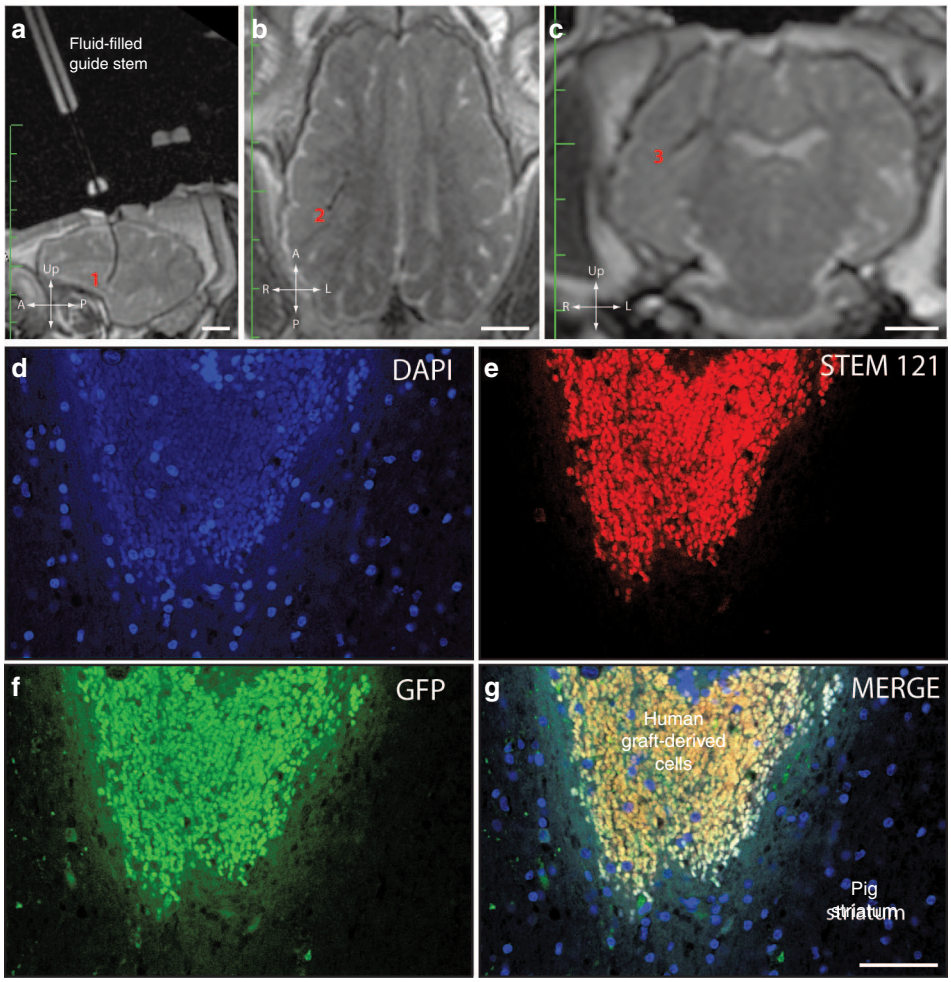

Figure 5 iMRI-guided RBD delivery of hDA cells to the swine striatum. (**a–c**) MRI scans obtained during the iMRI-guided RBD procedure. (**a**) Sagittal MRI showing anterior radial deployment (1) for hDA delivery. (**b**) Axial MRI showing posterolateral deployment (2). (**c**) Coronal MRI showing lateral and superior deployment. (**d–g**) IHC analysis of hDA cells grafted to the swine striatum. (**d**) 4',6-diamidino-2-phenylindole nuclear stain. (**e**) STEM121-positive cells at the graft site. (**f**) GFP-positive cells at the graft site. (**g**) IHC images merged showing the border between the graft-derived cells and the swine striatum. **a–c**, bar = 1 cm; **d–g**, bar = 100 µm. GFP, green fluorescent protein; IHC, immunohistochemistry; iMRI, interventional magnetic resonance image; RBD, radially branched deployment.

Furthermore, clinical-grade, human embryonic stem cell–derived dopamine neuronal precursor (hDA) cells (4×10^7 cells/ml)[36] also exhibited unchanged viability before (74.5 ± 1.3% SD; n = 3) and after (76.8 ± 1.2% SD; n = 3; t-test P = 0.29) device transit. Thus, the materials and mechanical properties of the RBD cell delivery catheter are not detrimental to neural precursor cells including those relevant to the treatment of PD.

We next evaluated the feasibility of delivering hDA cells with the iMRI-compatible RBD device. A total of 16 hDA cellular deposits (4×10^5 cells in a 10 µl volume delivered over 2 minutes) were implanted into the striatum of six swine (**Supplementary Table S3**). Some hDA cell populations were engineered to express green fluorescent protein[37,38] to facilitate the identification of graft-derived cells. In the surgeries performed with iMRI (eight separate deposits, three swine, **Supplementary Table S3**), proper cannula placement and catheter deployment was confirmed with rapid MRI scans immediately before cell delivery (**Figure 5a–c**). No hemorrhages were noted on iMRI scans, and all animals recovered from the RBD procedure without neurological deficits. Seven days after cell delivery, swine brains were analyzed by histology and immunohistochemistry. Immunohistochemistry for STEM 121 (human cytoplasmic antigen) and green fluorescent protein demonstrated human, graft-derived cells at the sites of cell implantation (**Figure 5d–g**). Thus, iMRI-guided RBD is a surgical platform that enables real-time targeting and monitoring for the delivery of human neural cells to large brain targets.

DISCUSSION

The development of the iMRI-guided RBD cell delivery platform was motivated by the observed technical limitations of devices and surgical strategies used in recent clinical trials. As with any therapeutic agent, effective delivery is critical to achieve a therapeutic effect,[1–3] and technical limitations at this final stage of clinical translational may contribute to the failure of human trials involving direct cell transplantation into the brain. The use of straight cannulas with standard stereotactic targeting has several important shortcomings related to the efficiency of cell distribution and transplantation accuracy.[3] By combining iMRI guidance

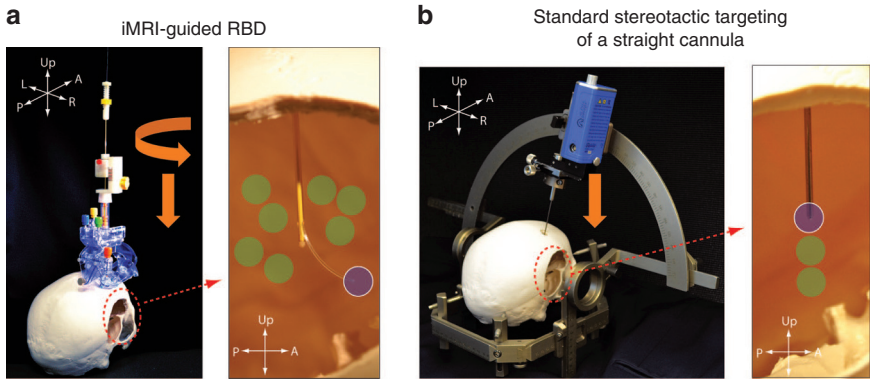

Figure 6 Illustration of advances provided by iMRI-guided RBD for cell transplantation into the brain. (**a**) iMRI-guided RBD. Targeting is performed with intraoperative MRI scans, which enables corrections for brain "shift," and delivery can be monitored in "real time" with rapid MRI scans. iMRI also provides intraoperative imaging for the early detection of potential complications such as hemorrhage. By controlling guide cannula radial angle and depth (orange arrows) and delivery catheter radial distance, cells (schematized as green and purple circles) can be delivered to larger brain target volumes that vary in shape and size due to individual patient anatomy and different disease states. (**b**) Standard stereotactic targeting of a straight cannula. Targeting is performed with preoperative MRI scans that are spatially registered to the skull mounted frame. Brain shift due to the loss of cerebrospinal fluid and the entry of air into the cranial vault can result in missed targets and the unintentional transgression of critical brain structures. With a straight cannula, cell delivery is limited to a single tract per cannula trajectory. iMRI, interventional magnetic resonance image; RBD, radially branched deployment.

with the control over three additional stereotactic parameters (radial angle, radial distance, and depth), this platform technology advances our ability to properly "tailor" cell delivery to larger brain target volumes that vary in shape and size due to individual patient anatomy and different disease states (**Figure 6**).

Straight cannula and syringe systems have been and are still widely used in clinical trials for cell transplantation to the brain.[8,12–16] This technology limits cell distribution to a single tract per initial brain penetration, and to accommodate the larger target volumes of the human brain, several transcortical brain penetrations have been required. For instance, some PD patients receiving cell transplants into the postcommisural putamen underwent 16 separate transcortical cannula insertions with standard targeting.[12] Although the neurosurgical risk of stereotactic cannula insertions is not well known, the incidence of hemorrhage with DBS electrode implantation through a straight cannula ranges from 0.9 to 12.8%.[17–19] With iMRI-guided RBD, we were able to place deposits in the entire putamen from a single guide cannula tract. Because imaging can be obtained immediately before and during cannula insertion, the avoidance of major blood vessels and sulci (which contain smaller fragile vessels) is technically more definitive than with standard stereotactic methods. Furthermore, if a hemorrhage were to occur during iMRI-guided RBD, this adverse event would be detected by imaging at the time of occurrence, thus enabling the early implementation of measures that can mitigate the complication (*e.g.*, termination of the remainder of the procedure, reduction in blood pressure). Thus, this platform technology has the potential of increasing patient safety.

Accuracy of cell delivery is likely crucial to cell transplantation efficacy. For instance, the variation in individual patient outcomes of past PD cell transplantation trials has been attributed in part to suboptimal targeting and cell dosing.[39,40] Based on our current understanding, dopamine cells should be grafted primarily to dopamine-deficient regions of the putamen and not to regions with sufficient dopaminergic input. Such brain targets can be accurately defined on preoperative MRI scans. However, after the dura is opened, brain structures can shift within the skull, reducing the accuracy of standard stereotactic targeting methods that assume no such change.[24,41] While cerebrospinal fluid egress can be minimized, reducing brain shift of deep brain structures,[42] the location of more superficial targets can be still significantly altered by dural opening. iMRI-guided RBD enables iterative, nearly real-time corrections to the targeting, and if the cells are labeled with MR-visible materials or coinfused with SPIO, the location of each cell deposit can be confirmed at the time of delivery.

Radial deployment of the delivery catheter in an agarose brain mimic was highly precise, and we did not notice differences in deployment characteristics when used in the human cadaveric brain. Thus, it appears that the material characteristics of the delivery catheter are sufficient to maintain a predictable deployment path despite potential differences in the modulus of the agarose gel and human cadaveric brain. In any case, catheter deployment in future live human brain could be monitored with iMRI, which allows for targeting corrections, if necessary.

The RBD concept includes a modular, "exchangeable" cell delivery catheter to provide greater control over cell dosing.[11] The iMRI-guided RBD platform makes such catheter exchange very simple. Given this aspect of the RBD device design, a separate cell delivery catheter can be used to dispense a cell aliquot that is specific to each radial location. In addition to enabling the delivery of specific cell numbers or volumes, even the cell type can be easily varied by the exchange of the cell delivery catheter subassembly. Furthermore, drugs or gene therapies can be directly infused through the radially deployed catheter or a similar subassembly with iMRI guidance.

One major goal of our work was to develop a platform technology that is both easy-to-use and has a low barrier to implementation. We therefore designed iMRI-guided RBD to function as an "add-on" to a currently available, skull-mounted aiming device and software package.[25] Importantly, this procedure does not require a specialized operating room but rather can be performed "inside" a typical 1.5T diagnostic MRI scanner covered

with a sterile drape. Furthermore, all of the neurosurgical and imaging procedures employed are essentially the same as that used for the iMRI-guided implantation of DBS electrodes. The use of depth, radial angle, and radial distance as new stereotactic parameters is intuitive, and the RBD control elements have been designed for clinical use (*e.g.*, their size and tactile feedback are compatible with the use of surgical gloves, and visual markings are clear and use common metric units). Because of this inherent ease-of-use and the widespread availability of 1.5T MRI scanners, iMRI-guided RBD for cell delivery can be implemented in most modern hospitals, which facilitates the conduct of multisite clinical trials and future adoption of successful cellular therapies for patient care worldwide.

Because this iMRI-guided RBD platform integrates easily into standard neurosurgical procedures that may ordinarily be performed in the patient care, the barrier to clinical trial development may be lower. For instance, the treatment of PD includes the implantation of DBS electrodes, which can be performed with iMRI.[25] At the same surgical session, it would be possible to deliver cells (or not, in study control patients) before DBS implantation through the same burr hole, aiming device, and software system. Because of this "piggyback" trial design, the procedural risk to the patient is essentially the same as a standard DBS therapy, which may lower concerns from regulatory bodies. Similarly, one can envisage iMRI-guided RBD delivery of cell or other biologics for the treatment of brain tumors at the time of iMRI-guided biopsy and diagnosis.

iMRI-guided RBD has not yet been used for the neurosurgical treatment of live human patients. Furthermore, the determination of proper cell dose delivered by iMRI-guided RBD per deployment site will likely require empiric testing for each specific cell type and brain target. However, the ongoing preclinical development of diverse cellular therapeutics for many important diseases of the brain will generate numerous opportunities for the in-human use of this platform technology. Future clinical trials performing intracerebral cell transplantation with iMRI-guided RBD may further demonstrate the inherent benefits of its technological advancements for neurosurgical stereotactic implantation procedures.

In summary, iMRI-guided RBD provides greater stereotactic freedom, enhanced targeting, and real-time monitoring for cell transplantation to the brain. By facilitating intracerebral cell delivery at the scale and complexity of the human brain, iMRI-guided RBD may have a transformative impact on the safety and efficacy of cellular therapeutics for a wide range of neurological disorders, helping ensure that basic science results are not lost in clinical translation.

MATERIALS AND METHODS

Device fabrication. All device materials are Medical Grade (**Table 1**), and the components were assembled in an EN ISO 13485:2003 certified facility (Second Source Medical, Palo Alto, CA). The outer guide tube (Victrex 381G fully crystalline PEEK), inner guide tube (Grilamid L25 Nylon 12 Natural), and delivery catheter (Grilamid L25 Nylon 12 Natural) were extruded, straightened via annealing and cut to length (MicroSpec, Peterborough, NH). The distal ends of all three components were made blunt by a tipping procedure, where a Teflon-coated mandrel, inserted into the lumen of each respective tube, was utilized to heat form a closed end. To scythe the distal side ports in both the inner and outer guide tubes, metal dies were designed in CAD software (Solidworks, Concord, MA) and fabricated. These fixtures enabled the side port to be cut by inserting a component into the respective fixture and rotating the tubing 360 degrees. A ramp was designed in Solidworks and fabricated (Grilamid L25 Nylon 12 Natural) by hand under a surgical scope. This was placed into the side port of the inner guide tube and fixed with an epoxy (Epotek 353 ND). Rounded fixtures (OD: 10.03 mm) formed by stereolithography (Accura-60; Fineline Prototyping, Raleigh, NC) were used to heat form the J-shape profile of the delivery catheter. Another fixture was formed (Second Source Medical) to hold the delivery catheter in position to scythe the distal infusion side port with a metal wire. Lastly, medical grade ink was used to mark the proximal end of the delivery catheter. The flexible end of the plunger wire was fabricated by adhering a Nitinol coiled wire to a tapered Nitinol wire. A piece of polyvinylidene fluoride (PVDF) was placed over the most distal end of the tapered Nitinol wire, heated with a heat shrink sheath to form a polymeric end and secured with an epoxy (Loctite 4061). To form a closed or blunt end, the tip of the plunger wire was trimmed, flattened, and tipped with an epoxy (Epotek 353NDT). Two polyurethane leaflet valves were adhered to the outer diameter of this epoxy tip to provide a better seal.

The RBD positioning collet is comprised of 29 thermoplastic parts that were formed by stereolithography (Accura-60; 3D Systems, Rock Hill, SC). In this version, the distal end of the collet contains a design element that secures this subassembly to the proximal end of the ClearPoint SmartFrame (MRI Interventions, Memphis, TN) guide cannula.

Assessment of cell delivery catheter deployment. Catheter deployment was evaluated in an agarose gel (Invitrogen, Life Technologies, Irvine, CA) cast within a clear acrylic box at a concentration (0.4%) that mimics the modulus (stiffness) of brain tissue. A SmartFrame with an attached positioning collet was mounted above the gel box, and this platform was used to insert the RBD outer guide tube subassembly 7 cm below the agarose surface. After the catheter-plunger subassembly was placed into the guide cannula, the side port was opened, and the catheter was deployed at various prescribed distances. Two cameras (Nikon D7000 with a Nikon AF-S DX Micro-Nikkor 40mm f/2.8G lens, Tokyo, Japan) stabilized with Pedco UltraPod II Lightweight Camera Tripods (Industrial Revolution, Tukwila, WA). were placed orthogonal to the samples, and at each deployment position, orthogonal images were obtained essentially simultaneously. Images were analyzed with Image-J (National Institutes of Health, Bethesda, MD).

Evaluation of volumetric precision of the delivery catheter. The cell delivery catheter was backfilled with distilled water, and the amount of water dispensed with each centimeter of plunger wire translational movement was determined by measuring the mass of the dispensed fluid on a precision analytic balance (AB54-S; Mettler Toledo, Columbus, OH).

Animal care. Seven female Yorkshire swine (age: 2.5–3 months; weight: 22–37.5 kg) underwent RBD procedures in this study (**Supplementary Table S3**). Experimentation was performed according to National Institutes of Health guidelines and to protocols approved by the Institutional Animal Care and Use Committee at the Veterans Affairs Medical Center (San Francisco, CA). All animals recovered without neurological deficits. One animal suffered from autopsy-confirmed, preexisting chronic pneumonia with abscesses and was euthanized 1 day after surgery. All other animals were allowed to survive 7 days after procedures. Vital signs and a standard veterinary neurological assessment including level of consciousness, behavior, cranial nerves, motor, sensory, locomotion, and coordination was performed at least daily by trained veterinary nurses.

RBD surgical procedure in swine. After premedication with ketamine (20 mg/kg), xylazine (2 mg/kg), and glycopyrrolate (0.01 mg/kg), the pig was intubated and ventilated with 1–4% isoflurane. The scalp was then sterilely prepped and draped, a midline scalp incision made, and a high-speed neurosurgical drill (Medtronic, Minneapolis, MN) with a perforator (ACRA-CUT, Acton, MA) was used to create a 12 mm burr hole centered

10 mm anterior and 7 mm lateral to bregma. After the dura and pia mater were opened, the base of ClearPoint SmartFrame was affixed with titanium screws over the burr hole. For iMRI-guided RBD, the pig was transferred to the clinical MRI suite under sterile drapes. A Hallowell EMC Model 2002 (Hallowell, Pittsfield, MA) ventilator was used, and vital signs were monitored throughout the procedure.

In the MRI suite, the pig was placed prone on the gantry of the 1.5T MRI scanner (Siemens Avanto, Erlangen, Germany), and the head was immobilized with a carbon-fiber skull fixation frame (MRI Interventions). The SmartFrame was then attached to its skull-mounted base, and volumetric T1-weighted and T2-weighted MRI scans were obtained (see **Supplementary Table S4** for parameters). MRI digital imaging and communications in medicine (DICOM) data were transferred via a standard network connection to the ClearPoint workstation, which exists as a standalone laptop computer. The swine anterior commissure, posterior commissure, and midsagittal plane were identified and registered to provide a spatial reference for target coordinates, with the center being the intersect between the anterior commissure, posterior commissure, and midsagittal planes. The MRI-visible (gadolinium-impregnated) SmartFrame fiducials and gadolinium fluid-filled stem guide were also identified and registered to this space. By establishing coordinates for the initial guide cannula target and the cortical entry point, a trajectory for the guide cannula insertion was determined.

To adjust the SmartFrame fluid stem guide tube to match the desired guide cannula trajectory, rapid MRI scans (**Supplementary Table S4**) were used in manner essentially as previously described. Briefly, the pitch and roll of the SmartFrame were adjusted iteratively with imaging feedback from rapid MRI scans. When the expected error was less than 1.0 mm, the pitch and roll axes on the SmartFrame were locked. Then, the X-Y platform was adjusted in a similar manner until the expected error was less than 0.5 mm, which typically required no more than two iterations. With the fluid-filled stem guide locked in the final position, the Z-distances (depth) along the guide cannula trajectory could be determined. From this planned guide cannula trajectory, RBD depths, radial angles, and radial distances could be calculated. The guide cannula subassembly was then inserted through the positioning collet, and the Z-depth control wheel and radial angle adjustment hub were used to bring the side port to the desired initial depth and radial angle. After confirming the guide tube placement with rapid MRI scans, the delivery catheter was backfilled with the desired suspension and loaded in the guide tube. After opening the guide cannula side port, the delivery catheter was deployed, and rapid MRI scans were used to verify the catheter location. After verifying the correct catheter location, the SPIO (superparamagnetic iron oxide beads, 10 µm diameter; Bang Laboratories, Fishers, IN) suspension (10 µl; 0.16 mg/ml) or hDA cells (10 µl; 4×10^7 cells/ml) was delivered via manual translation of the integrated plunger-wire over the course of 2.5 minutes. The location of each SPIO deposit was confirmed immediately after delivery. After removal of the spent delivery catheter and closure of the side port, the positioning collet controls were used to bring the side port to the next desired depth and radial angle, and radial deployment and delivery was performed again as described above. After completing all planned radial deliveries, 2D spin-echo MR images were acquired that were equivalent to the baseline T2-weighted scans. The aiming device was then removed from the skull, and the scalp was closed with nylon sutures. The animals were then extubated and allowed to recover under close observation until they were able to right themselves in their home cages. DICOM data obtained during iMRI-guided RBD procedures were analyzed with OsiriX, an open-source DICOM reader and imaging software package (http://www.osirix-viewer.com).

Brain histology. After the pig was euthanized, the brain was removed via a large craniotomy, sectioned into 10–15 mm coronal blocks with a brain matrix, fixed in 4% paraformaldehyde for 7 days at 4 °C, then saturated with 30% (w/v) sucrose for 7–10 days at 4 °C. A freezing-sliding microtome (Fisher Scientific, Philadelphia, PA) was used to cut 40-µm serial sections for histological processing. For immunohistochemisty, sections were first treated with 1% H_2O_2, blocked with 5% goat serum in phosphate-buffered saline with 0.1% Tween-20, then incubated overnight at 4 °C with primary mouse anti-human cytoplasmic marker (STEM121; StemCells, Newark, CA), or chicken antigreen fluorescent protein antibody (AVES Labs, Tigard, OR) diluted at 1:500 with blocking buffer. Alexa Fluor 488 goat antichicken or Alexa Fluor 594 goat antimouse secondary antibody (Invitrogen, Grand Island, NY) was used to detect the primary antibodies. The omission of primary antibody served as a negative control. Images were acquired with a Leica CTR 6500 confocal microscope (Leica Microsystems, Wetzlar, Germany).

iMRI-guided RBD in human cadaveric heads. The MRI-guided RBD delivery of SPIO into three cadaveric heads was performed using the ClearPoint system as described above. After the base of the SmartFrame was mounted on the skull, the head was secured to the MR gantry with a neurosurgical head fixation frame (Malcolm-Rand; CMI Composites, San Clemente, CA). Imaging was performed on an Achieva 1.5T MR system (Philips, Cleveland, OH) with scanning parameters as in **Supplementary Table S6**. The RBD procedure was performed essentially as described above for live swine surgery. The distribution and spatial patterns of SPIO delivery was analyzed with OsiriX (http://www.osirix-viewer.com).

Analysis of cell viability. Cell viability before and after their passage through the RBD delivery catheter was performed as previously described.[11] Briefly, the cell delivery catheter was backfilled with 50 µl of each cell suspension and dispensed into a polystyrene test tube at a rate of 5 µl/minutes. Dead cells were stained with Sytox Red (Life Technologies, Grand Island, NY) and quantified via flow cytometry (LSR II; BD Bio-sciences, San Jose, CA).

Cell culture. hDA cells for transplantation were generated with a GMP-compatible process from neural stem cells derived from the H14 ESC line as previously described.[36,43] Briefly, neural stem cells were plated on poly-ornithine-laminin–coated culture dishes in STEMPRO medium (DMEM/F-12+GLUTAMAXTM medium with STEMPRO hESC SFM Growth Supplement, 1.8% bovine serum albumin, and 8 ng/ml FGF2) supplemented with sonic hedgehog (200 ng/ml), BMP2 (4 ng/ml), and activin A (10 ng/ml). Ten days after differentiation, cells were differentiated in STEMPRO medium supplemented with brain derived neurotrophic factor (20 ng/ml), glial cell-line derived neurotrophic factor (20 ng/ml), dibutyryl cyclic adenosine 3',5'-monophosphate (0.1 mmol/l), and activin A (10 ng/ml) for 4 days and cryopreserved for transplantation. At this stage (day 14 transplantable dopaminergic precursor/neuron), ~70% of total cells expressed midbrain dopaminergic markers Lmx1A and FoxA2, and less than 5% of total cells expressed TH.

Murine neural stem cells were generated from the postnatal mouse brain as previously described.[44] Briefly, subventricular zone tissue from the brains of P7 to P9 mice were dissociated with 0.25% trypsin and trituration. Cells were grown in proliferation medium (DMEM/F12/N2, Invitrogen; 5% fetal calf serum; epidermal growth factor (20 ng/ml); basic fibroblast growth factor (20 ng/ml); and bovine pituitary extract (35 µg/ml). Cells were passaged 1:2 with 0.25% trypsin.

SUPPLEMENTARY MATERIAL

Figure S1. Example of a frame-based platform for standard stereotactic targeting of a straight cannula.
Figure S2. Deployment of the delivery catheter along a smooth path.
Figure S3. RBD positioning collet control mechanisms for guide cannula side port depth and radial angle.
Table S1. OD of commonly used cannulas for intracerebral cell transplantation or DBS.
Table S2. Precision of delivery catheter deployment.
Table S3. Summary of swine study.
Table S4. MRI scan parameters (Siemens 1.5-T) for swine studies.

Table S5. Summary of cadaveric head study.
Table S6. MRI scan parameters (Philips Achieva 1.5-T) for human cadaveric head studies.

ACKNOWLEDGMENTS

This work was supported by a California Institute for Regenerative Medicine (CIRM) Tools and Technology award RT2-01975 and the NIH Director's New Innovator Award 1DP2OD006505-01 to D.A.L.
M.T.S., T.A.D., and D.A.L. contributed to the overall design, manufacturing, and testing of the device. A.J.M. provided MRI scanner expertise for all iMRI procedures. D.Y., M.T.S., D.A.L., V.G.C., P.M., and S.S.P. performed the swine experiments. M.T.S. and D.Y. performed human cadaveric head experiments. P.S.L., P.A.S., and N.G. are neurosurgeons who consulted on device design and workflow. X.Z. provided hDA cells for testing and experimental design of hDA cell transplantation. D.A.L. wrote the manuscript, and all authors provided critical input.
The Regents of the University of California with M.T.S., T.A.D., and D.A.L. as coinventors have filed a patent application that includes the iMRI-guided RBD technology.

REFERENCES

1. Mooney, DJ and Vandenburgh, H (2008). Cell delivery mechanisms for tissue repair. *Cell Stem Cell* **2**: 205–213.
2. Soto-Gutierrez, A, Yagi, H, Uygun, BE, Navarro-Alvarez, N, Uygun, K, Kobayashi, N *et al.* (2010). Cell delivery: from cell transplantation to organ engineering. *Cell Transplant* **19**: 655–665.
3. Potts, MB, Silvestrini, MT and Lim, DA (2013). Devices for cell transplantation into the central nervous system: design considerations and emerging technologies. *Surg Neurol Int* **4** (suppl. 1): S22–S30.
4. Aboody, K, Capela, A, Niazi, N, Stern, JH and Temple, S (2011). Translating stem cell studies to the clinic for CNS repair: current state of the art and the need for a Rosetta stone. *Neuron* **70**: 597–613.
5. Brecknell, JE and Fawcett, JW (1996). A device for the implantation of multiple cellular deposits into a large volume of brain from a single cannula site. *Exp Neurol* **138**: 338–344.
6. Bankiewicz, KS, Bringas, J, Pivirotto, P, Kutzscher, E, Nagy, D and Emborg, ME (2000). Technique for bilateral intracranial implantation of cells in monkeys using an automated delivery system. *Cell Transplant* **9**: 595–607.
7. Mendez, I, Hong, M, Smith, S, Dagher, A and Desrosiers, J (2000). Neural transplantation cannula and microinjector system: experimental and clinical experience. Technical note. *J Neurosurg* **92**: 493–499.
8. Kondziolka, D, Steinberg, GK, Cullen, SB and McGrogan, M (2004). Evaluation of surgical techniques for neuronal cell transplantation used in patients with stroke. *Cell Transplant* **13**: 749–754.
9. Cunningham, MG, Bolay, H, Scouten, CW, Moore, C, Jacoby, D, Moskowitz, M *et al.* (2004). Preclinical evaluation of a novel intracerebral microinjection instrument permitting electrophysiologically guided delivery of therapeutics. *Neurosurgery* **54**: 1497–507; discussion 1507.
10. Bjarkam, CR, Glud, AN, Margolin, L, Reinhart, K, Franklin, R, Deding, D *et al.* (2010). Safety and function of a new clinical intracerebral microinjection instrument for stem cells and therapeutics examined in the Göttingen minipig. *Stereotact Funct Neurosurg* **88**: 56–63.
11. Silvestrini, MT, Yin, D, Coppes, VG, Mann, P, Martin, AJ, Larson, PS *et al.* (2013). Radially branched deployment for more efficient cell transplantation at the scale of the human brain. *Stereotact Funct Neurosurg* **91**: 92–103.
12. Breeze, RE, Wells, TH Jr and Freed, CR (1995). Implantation of fetal tissue for the management of Parkinson's disease: a technical note. *Neurosurgery* **36**: 1044–7; discussion 1047.
13. Freed, CR, Greene, PE, Breeze, RE, Tsai, WY, DuMouchel, W, Kao, R *et al.* (2001). Transplantation of embryonic dopamine neurons for severe Parkinson's disease. *N Engl J Med* **344**: 710–719.
14. Olanow, CW, Goetz, CG, Kordower, JH, Stoessl, AJ, Sossi, V, Brin, MF *et al.* (2003). A double-blind controlled trial of bilateral fetal nigral transplantation in Parkinson's disease. *Ann Neurol* **54**: 403–414.
15. Mendez, I, Sanchez-Pernaute, R, Cooper, O, Viñuela, A, Ferrari, D, Björklund, L *et al.* (2005). Cell type analysis of functional fetal dopamine cell suspension transplants in the striatum and substantia nigra of patients with Parkinson's disease. *Brain* **128** (Pt 7): 1498–1510.
16. Barker, RA. (2013). TRANSEURO open label transplant study in Parkinson's disease. https://Clinical Trials.gov.
17. Deep-Brain Stimulation for Parkinson's Disease Study Group. Deep-brain stimulation of the subthalamic nucleus or the pars interna of the globus pallidus in Parkinson's disease. *N Engl J Med* **345**: 956–963 (2001).
18. Binder, DK, Rau, GM and Starr, PA (2005). Risk factors for hemorrhage during microelectrode-guided deep brain stimulator implantation for movement disorders. *Neurosurgery* **56**: 722–32; discussion 722.
19. Zrinzo, L, Foltynie, T, Limousin, P and Hariz, MI (2012). Reducing hemorrhagic complications in functional neurosurgery: a large case series and systematic literature review. *J Neurosurg* **116**: 84–94.
20. Bobo, RH, Laske, DW, Akbasak, A, Morrison, PF, Dedrick, RL and Oldfield, EH (1994). Convection-enhanced delivery of macromolecules in the brain. *Proc Natl Acad Sci USA* **91**: 2076–2080.
21. Murad, GJ, Walbridge, S, Morrison, PF, Szerlip, N, Butman, JA, Oldfield, EH *et al.* (2007). Image-guided convection-enhanced delivery of gemcitabine to the brainstem. *J Neurosurg* **106**: 351–356.
22. Barua, NU, Gill, SS and Love, S (2014). Convection-enhanced drug delivery to the brain: therapeutic potential and neuropathological considerations. *Brain Pathol* **24**: 117–127.
23. Subramanian, T, Deogaonkar, M, Brummer, M and Bakay, R (2005). MRI guidance improves accuracy of stereotaxic targeting for cell transplantation in parkinsonian monkeys. *Exp Neurol* **193**: 172–180.
24. Pallavaram, S, Dawant, BM, Remple, MS, Neimat, JS, Kao, C, Konrad, PE *et al.* (2010). Effect of brain shift on the creation of functional atlases for deep brain stimulation surgery. *Int J Comput Assist Radiol Surg* **5**: 221–228.
25. Larson, PS, Starr, PA, Bates, G, Tansey, L, Richardson, RM and Martin, AJ (2012). An optimized system for interventional magnetic resonance imaging-guided stereotactic surgery: preliminary evaluation of targeting accuracy. *Neurosurgery* **70**(1 Suppl Operative): 95–103; discussion 103.
26. Lim, DA & Larson, PS. (2009). *Intraoperative MRI in Functional Neurosurgery*. Elsevier: Philadelphia. pp. 237.
27. Martin, AJ, Hall, WA, Roark, C, Starr, PA, Larson, PS and Truwit, CL (2008). Minimally invasive precision brain access using prospective stereotaxy and a trajectory guide. *J Magn Reson Imaging* **27**: 737–743.
28. Ostrem, JL, Galifianakis, NB, Markun, LC, Grace, JK, Martin, AJ, Starr, PA *et al.* (2013). Clinical outcomes of PD patients having bilateral STN DBS using high-field interventional MR-imaging for lead placement. *Clin Neurol Neurosurg* **115**: 708–712.
29. Starr, PA, Martin, AJ and Larson, PS (2009). Implantation of deep brain stimulator electrodes using interventional MRI. *Neurosurg Clin N Am* **20**: 193–203.
30. Starr, PA, Martin, AJ, Ostrem, JL, Talke, P, Levesque, N and Larson, PS (2010). Subthalamic nucleus deep brain stimulator placement using high-field interventional magnetic resonance imaging and a skull-mounted aiming device: technique and application accuracy. *J Neurosurg* **112**: 479–490.
31. Gobbel, GT, Kondziolka, D, Fellows-Mayle, W and Uram, M (2010). Manual vs automated delivery of cells for transplantation: accuracy, reproducibility, and impact on viability. *Neurosurgery* **67**: 1662–8; discussion 1668.
32. Maciunas, RJ, Galloway, RL Jr and Latimer, JW (1994). The application accuracy of stereotactic frames. *Neurosurgery* **35**: 682–94; discussion 694.
33. Bjartmarz, H and Rehncrona, S (2007). Comparison of accuracy and precision between frame-based and frameless stereotactic navigation for deep brain stimulation electrode implantation. *Stereotact Funct Neurosurg* **85**: 235–242.
34. Sauleau, P, Lapouble, E, Val-Laillet, D and Malbert, CH (2009). The pig model in brain imaging and neurosurgery. *Animal* **3**: 1138–1151.
35. Yin, D, Valles, FE, Fiandaca, MS, Forsayeth, J, Larson, P, Starr, P *et al.* (2009). Striatal volume differences between non-human and human primates. *J Neurosci Methods* **176**: 200–205.
36. Liu, Q, Pedersen, OZ, Peng, J, Couture, LA, Rao, MS and Zeng, X (2013). Optimizing dopaminergic differentiation of pluripotent stem cells for the manufacture of dopaminergic neurons for transplantation. *Cytotherapy* **15**: 999–1010.
37. Zeng, X, Cai, J, Chen, J, Luo, Y, You, ZB, Fotter, E *et al.* (2004). Dopaminergic differentiation of human embryonic stem cells. *Stem Cells* **22**: 925–940.
38. Macarthur, CC, Xue, H, Van Hoof, D, Lieu, PT, Dudas, M, Fontes, A *et al.* (2012). Chromatin insulator elements block transgene silencing in engineered human embryonic stem cell lines at a defined chromosome 13 locus. *Stem Cells Dev* **21**: 191–205.
39. Dunnett, SB, Björklund, A and Lindvall, O (2001). Cell therapy in Parkinson's disease - stop or go? *Nat Rev Neurosci* **2**: 365–369.
40. Lindvall, O and Björklund, A (2004). Cell therapy in Parkinson's disease. *NeuroRx* **1**: 382–393.
41. Miyagi, Y, Shima, F and Sasaki, T (2007). Brain shift: an error factor during implantation of deep brain stimulation electrodes. *J Neurosurg* **107**: 989–997.
42. Petersen, EA, Holl, EM, Martinez-Torres, I, Foltynie, T, Limousin, P, Hariz, MI *et al.* (2010). Minimizing brain shift in stereotactic functional neurosurgery. *Neurosurgery* **67**(3 Suppl Operative): ons213–21; discussion ons221.
43. Peng, J, Liu, Q, Rao, MS and Zeng, X. (2014). Survival and engraftment of dopaminergic neurons manufactured by a GMP-compatible process. *Cytotherapy* **16**: 1305–1312.
44. Hwang, WW, Salinas, RD, Siu, JJ, Kelley, KW, Delgado, RN, Paredes, MF *et al.* (2014). Distinct and separable roles for EZH2 in neurogenic astroglia. *Elife* **3**: e02439.